

Ultrasonic and Numerical Modeling of Reflections from Simulated Fractured Reservoirs

Stephen Theophanis (theophanis@srl.com; 617-547-1122)
Science Research Laboratory
15 Ward Street
Somerville, MA 02143

Xiang Zhu (xzhu@erl.mit.edu; 617-253-1422)
Earth Resources Laboratory / Massachusetts Institute of Technology
42 Carleton Street
Cambridge, MA 02142

Abstract

In order to develop modeling techniques for the characterization of fracture properties in tight gas sands from surface seismic reflection data we examine seismic waves scattered from anisotropic heterogeneity with laboratory data and numerical modeling. Laboratory models representing features of a fractured reservoir were constructed using Phenolite (the “reservoir”) embedded in a Lucite background, and seismic surveys were gathered over these models. In parallel with laboratory measurements, finite-difference modeling of reflections from a fractured medium were carried out. Fracture zone properties were calculated using an effective medium theory, the variation of fracture density produced a heterogeneous medium. The heterogeneity was modeled with a stochastic process, characterized by a probability density function and an auto-correlation function. Results from both modeling efforts show that prestacked AVO data can contain important information describing reservoir heterogeneity.

Introduction

Natural fracturing is known to be a critical factor in production of gas from tight sands reservoirs. Effective production from such reservoirs requires methods for quickly and accurately analyzing fracture distributions, since *in situ* fracturing can control movement of gas within the reservoir. An efficient method for locating and characterizing fractured reservoirs is through the use of exploration seismology. The fractured areas within the reservoir are known to be the cause of very important seismic wave propagation phenomena. This is largely because in many areas, the least principal stress has a horizontal orientation. The result of this stress configuration is that open fractures in the rock formations typically have an overall parallel alignment. This creates a propagation medium which is *effectively anisotropic* even though the intrinsic material containing the fractures may be isotropic. Theoretical models and field observations of media containing aligned fractures confirm that the material is transversely isotropic, with a horizontal axis of symmetry (Hudson, 1980, 1981; Crampin, 1981; Crampin et al, 1986; Schoenberg and Douma, 1988; Leary et al., 1987). Such a rock formation will have distinctive variations of seismic wave velocity with direction.

The immediate objective of our current research is to develop fast numerical modeling techniques which will accurately predict the effects of fracture induced anisotropy of realistic scale and distribution on surface seismic data. To help accomplish this goal we have

constructed ultrasonic scale models containing simulated fractured reservoirs and conducted reflection surveys over these models. We have also conducted numerical calculations of wave fields for analogous models using the finite difference method. The results from these two modeling techniques allow us to directly compare the measured and calculated seismic responses to the known character of the simulated reservoirs. In this paper we present some preliminary results from these two modeling efforts.

Sub-Scale Ultrasonic Experiment

Ultrasonic scale laboratory models containing features of a fractured reservoir were constructed using Phenolite (the “reservoir”) embedded in a Lucite background. Phenolite displays azimuthal anisotropy analogous to that associated with formations containing aligned fractures. Three physical models were constructed to compare the P-wave seismic response of the commonly-assumed welded half-space (model 1) with more complicated reservoir geometries. The second model was constructed with a 0.5 cm thick Phenolite disk, 10 cm in diameter, which was designed for observing the effects of thin layers on AVOA data. The third model was constructed with 0.5 cm thick random width strips of Phenolite arranged on random centers to produce heterogeneity in one dimension. This model was designed to simulate the effects of reservoir heterogeneity caused by fracture swarms in AVOA data. The three individual model geometries are sketched in Figure 1.

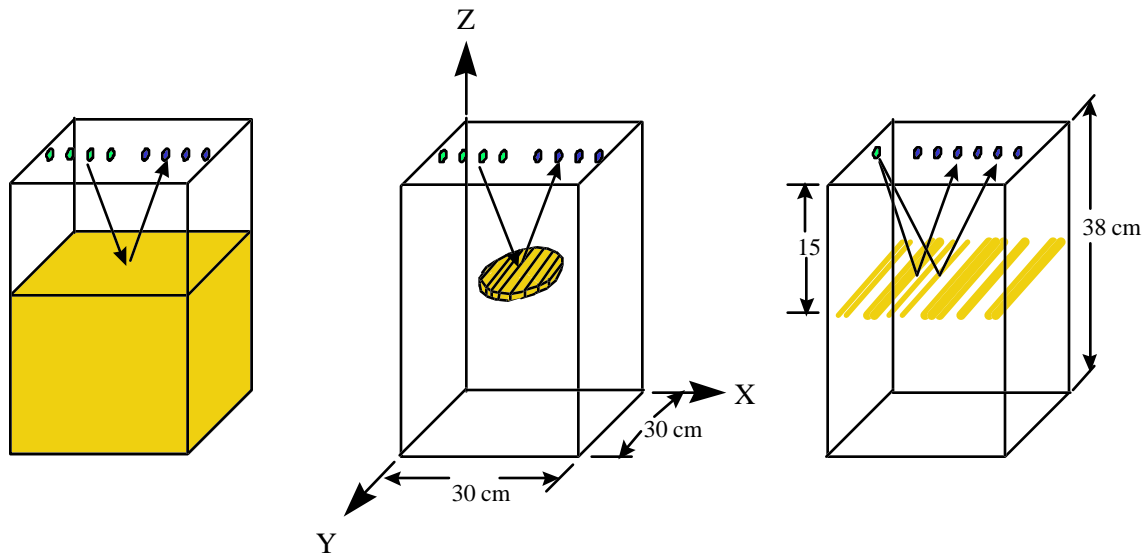


Figure 1. The three physical models, 1. (left) the welded half-space model, 2. (center) the thin disk model, 3. (right) the random medium model

Each ultrasound model was constructed of blocks of Lucite and pieces of Phenolite XX-324, a composite anisotropic material with orthorhombic symmetry, bonded with epoxy to dimensions of $30 \times 30 \text{ cm}^2$ by 38 cm in height. Lucite was chosen as the background material because it is homogeneous and isotropic. The epoxy bonding of all joints was performed under a uniform

pressure of 15 psi. The reflection coefficient for the epoxy joints between Lucite layers was tested with both P and S-waves of the appropriate frequencies and found to be unmeasurably small. The horizon representing the fractured reservoir is embedded 15 cm from the surface.

In each model the Phenolite layer is bonded to the Lucite background material, aligned with its “slow” axis parallel to the models' x-axis, using the epoxy bonding technique described earlier to ensure that reflections from the layer are not influenced by the joint. The physical properties of Phenolite are listed in Table 1, and Lucite values are: P-wave velocity 2750 m/s, S-wave velocity 1376 m/s, density 1190 kg/m³.

Property	Phenolite XX-324 value
C ₁₁	10.1 GPa
C ₁₂	7.9
C ₁₃	7.3
C ₂₂	17.5
C ₂₃	11.5
C ₃₃	20.8
C ₄₄	5.1
C ₅₅	2.63
C ₆₆	2.63
Density	1340 (kg/m ³)

Table 1. Physical properties of Phenolite

In conjunction with the sound speeds and feature sizes in the model, ultrasonic transducers of the appropriate frequency were chosen to produce an acoustic wavelength (~2 cm) scaleable to seismic exploration in the earth. This wavelength corresponds to a center frequency of approximately 200 kHz for P-waves. Conveniently this frequency range is close to that of conventional non-destructive testing (NDT) instrumentation. 1.0 inch diameter P-wave contact transducers were purchased from Panametrics, Waltham, MA. The center frequency and bandwidth of these transducers are adjustable within limits. The excitation pulse was provided by a Hewlett Packard 214B high voltage pulse generator which has independent control of voltage, pulse width and repetition rate. Data were collected directly from the receiving transducer with a Lecroy 9304A oscilloscope which has real time signal averaging capability for noise reduction and a disk drive for data storage.

Tuning of the source functions to optimize the center frequency and bandwidth was performed for the P-wave transducers by adjusting the source transducer's excitation pulse width. The windowed source signal, after propagation through 15 cm of Lucite, and its spectrum are plotted in Figure 2.

CMP reflection data were gathered over the welded half-space and disk models and shot gathers were conducted over the random medium model, all with offsets which ranged from 5 to 25 cm and array orientations at azimuths of 0 and 90 degrees (0 degrees is along the x-axis in Fig. 1). The incident angle of reflection at the Phenolite interface ranges from 10 to 40 degrees. Data were taken with the 200 kHz P-wave transducers. Each recorded trace was the result of 100 temporal averages, the noise reduction gained by the averaging negated the need for amplification which can cause signal distortion at the oscilloscope.

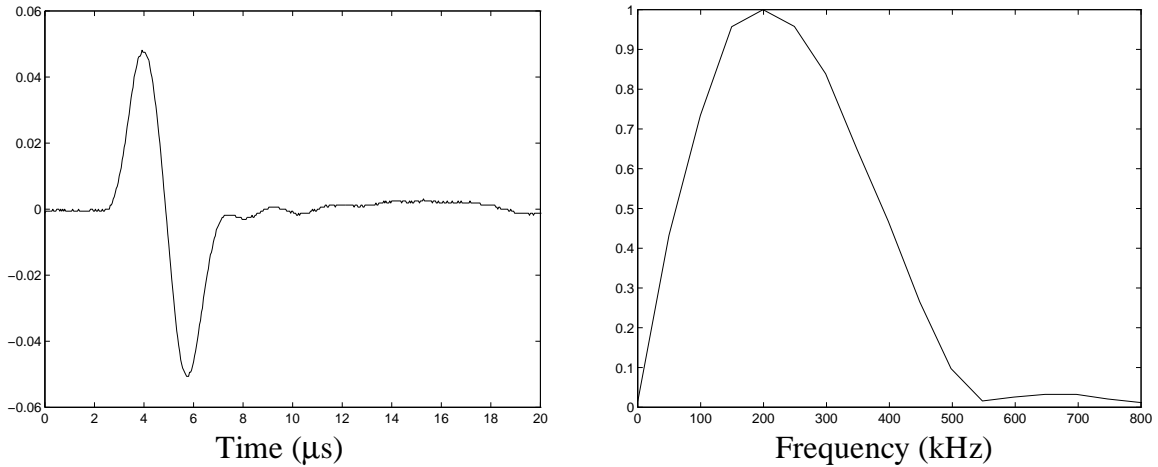


Figure 2: The P-wave source functions in both the time and frequency domains respectively

Examples of the seismic sections collected over the physical models are displayed in Figure 3. These sections were collected over the welded half-space model on the two principal azimuths using CDP gathers. Notice the surface Rayleigh wave starting at approximately 20 μs for near normal incidence, and the reflected wavelet of interest at approximately 110 μs.

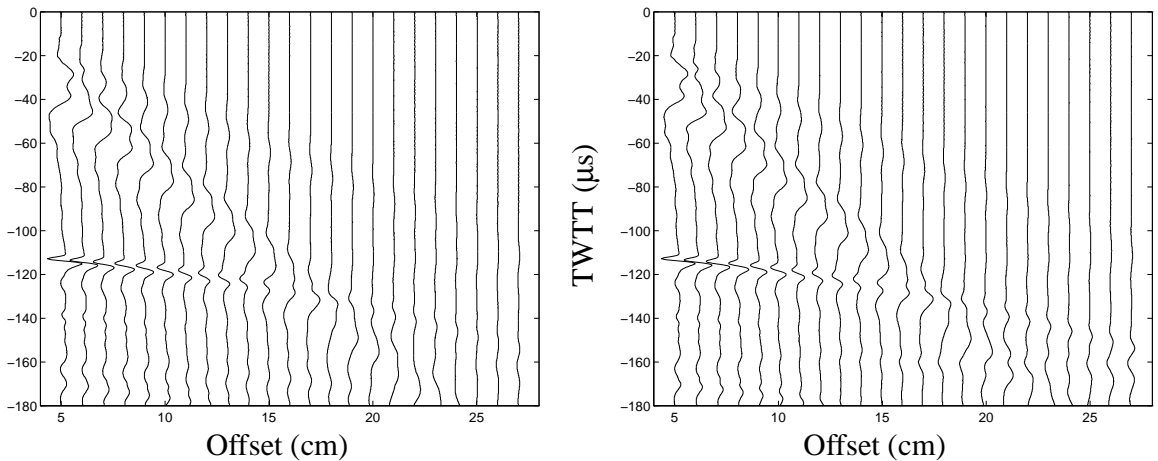


Figure 3. Seismic sections shot over the welded half-space model, the left-hand section is shot along azimuth=0°, at the right is azimuth=90°

In these traces, the wavelet amplitude fall-off with offset is quite severe, this is a result of the highly directional beam pattern associated with the ultrasonic transducers. This effect, along with propagation losses in the Lucite are compensated for in the AVO plots which are to follow. The compensation is accomplished by calculating a reference AVO function from data shot over a 15 cm thick Lucite model with reflections off the bottom free surface. Since we can

easily calculate the AVO for P-wave reflections off a free surface, we can calibrate the reference AVO function so that it contains only wavelet amplitudes associated with the transducers' beam pattern and propagation through the Lucite background. Raw AVO data gathered over our physical models are then adjusted using the reference AVO function which yields amplitudes as reflection coefficients of the simulated reservoir.

Figure 4 contains the AVO plots corresponding to the seismic sections in Figure 3 calculated using the procedure described above. The large amplitude spike starting at offset=0.2 is caused by the interference of the surface wave in the time window used to calculate the reflected wavelet's rms amplitude. We see evidence of AVO contrast between the two principal azimuths at far offset as a result of the lower medium's velocity anisotropy. Since we are most interested with this contrast, we calculate the difference between the two AVO curves which also nearly cancels the effect of the surface wave.

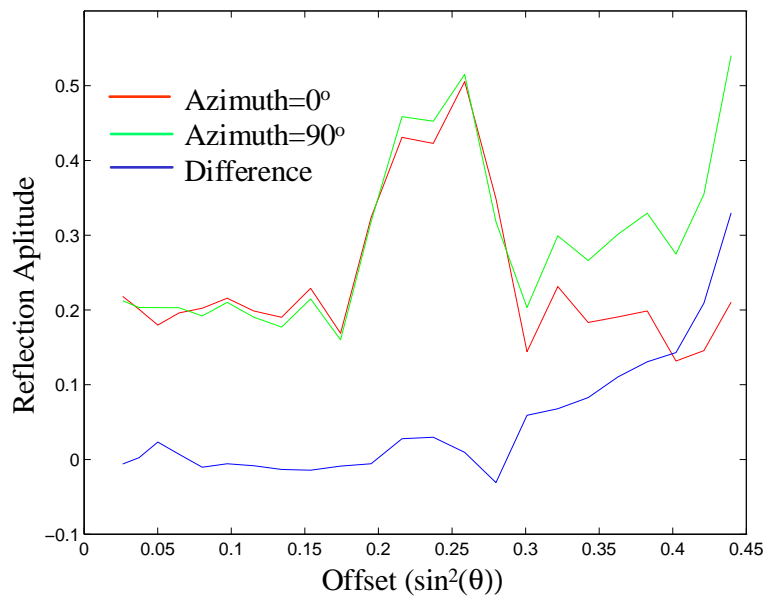


Figure 4. AVO curves for the two principal azimuths and their difference for data gathered over the welded half-space model

This result is of interest because we see that the difference curve starts at zero for normal incidence, which is expected, but it increases non-linearly with the sin squared of the incident angle.

To verify that this result is valid, we compare the measured AVO difference curve with one calculated using the appropriate material parameters (Figure 5).

Since there is a reasonably good correspondence between these two AVO difference curves we conclude that data gathered over the ultrasonic models and the processing techniques used yield results which can be considered reliable. The non-linear AVO result is caused by the relatively strong, Lucite/Phenolite normal incidence reflection coefficient (~20%), and the Phenolite anisotropy (~30%).

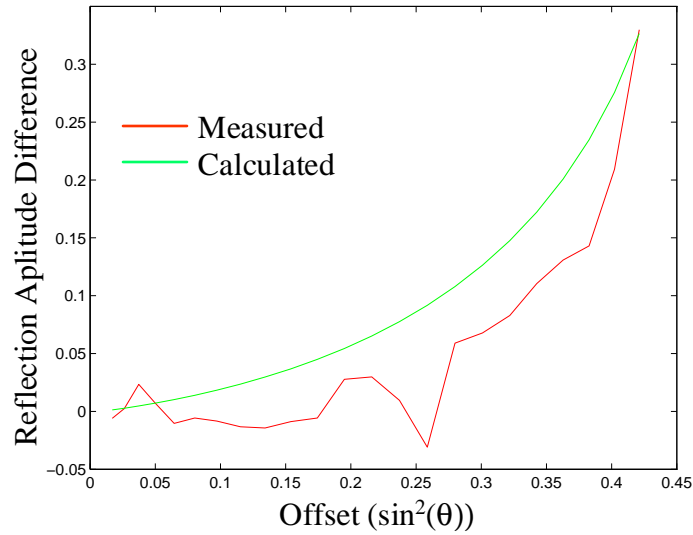


Figure 5. AVO difference curves for measured and calculated data from the welded half-space model

AVO results for the two principal azimuths shot over the thin disk model are displayed in Figure 6. Recall that the thin disk is made of the same material and its anisotropy is oriented in the same direction as the lower layer of the welded half-space model. Comparing these AVO curves with the ones in Figure 4, we once again see the effect of the surface wave, but in this case there is a dramatic loss of contrast (shown in the difference curve) between the two azimuths at far offset.

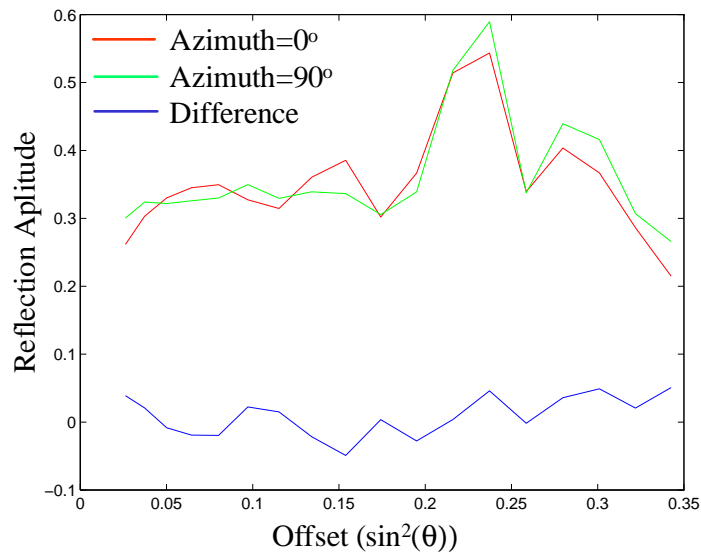


Figure 6. AVO curves for the two principal azimuths and their difference for data gathered over thin disk model

The best explanation for this loss of AVO contrast between the two azimuths is tuning effects. For a thin layer there exists a composite reflection coefficient which is frequency dependent interacting with the broadband source wavelet. At the frequency where the wavelength in the layer is twice that of the layer thickness there is a null in the reflection coefficient spectrum. Since the layer in our case is anisotropic, the wavelength in the layer varies differently with offset for the two principal azimuths. Therefore, the position of the reflection coefficient null in frequency space will be displaced for one azimuth relative to the other. Depending on the impedance mismatch of the material combinations and the bandwidth of the source wavelet, this effect can enhance or cancel, as in our case, the P-wave AVO contrast produced by the anisotropy.

For the random medium model it is important to recall that the seismograms were collected using a shot gather (illustrated in Figure 1) as opposed to CDP gathers used for the other two models. The motivation for this change is to attempt to infer the heterogeneous properties of the random medium model in the AVO curves.

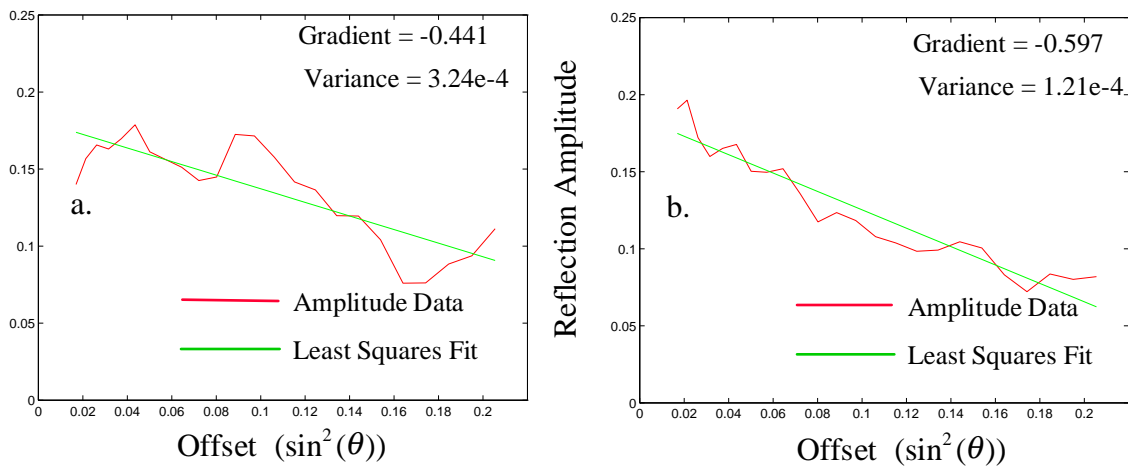


Figure 7. AVO curves for data gathered over the random media model, a. azimuth=0°, b. azimuth=90°

The AVO responses for the random medium model (Figure 7) display contrast between the two principal azimuths but not only in the conventional sense of a change in gradient. We also calculated the variance from a least-squares fit of the AVO curve, and found that the variance in the cross-line direction is nearly a factor of 3 greater than in the in-line direction. This experiment demonstrates the effect of small-scale heterogeneity on AVO data, in the follow section we describe how these data may be used to infer the heterogeneity of the reflecting layer.

Finite Difference Modeling

Using the finite difference method we study reflections from fractured reservoirs where fracturing introduces random heterogeneity with the following constraints: the heterogeneous parameter varies smoothly, its deviation from the mean is small, and it is stationary in space. With these assumptions, the heterogeneity can be modeled with a stationary stochastic process. Two functions characterize such a stochastic process, the probability density function and an auto-correlation function. The probability density function describes the mean value and

perturbation strength of the model parameters. Any probability density function can be considered a zero-mean function superposed on a constant, where the constant corresponds to the homogeneous reference background and the zero-mean function describes the deviation of the model parameters from the background. The probability density function is assumed to be Gaussian. The auto-correlation function describes the heterogeneity spatial scale and smoothness of the model and can be set to either, the Gaussian function, the exponential function or the von Karman function. These functions differ in the fall-off rate of high wavenumber components. Spectra with more energy at high wave-numbers are expected to show more roughness than those which are localized at low wave-numbers.

For our study, the medium is heterogeneous only in velocity, both the probability density function and the spatial auto-correlation function are set to Gaussians. The standard deviation parameter in the Gaussian spatial auto-correlation function is the distance where the correlation falls by one e-fold, which defines the correlation length.

The numerical model, analogous to the random medium physical model, consists of a homogeneous overburden and a heterogeneous layer with variable P-wave velocity in one lateral dimension. The model width is 1000 m, the homogeneous overburden velocity is 3000 m/s, the heterogeneous layer is 500 m below the surface, and its mean velocity is 5000 m/s. The model grid spacing is 5 m in both the x and z directions. Velocity perturbation in the heterogeneous layer is held within 10% of the mean value. Several runs were made varying the spatial auto-correlation length in the range from 25 m (1/4 wavelength) to 200 m (2 wavelengths) as shown in Figure 8.

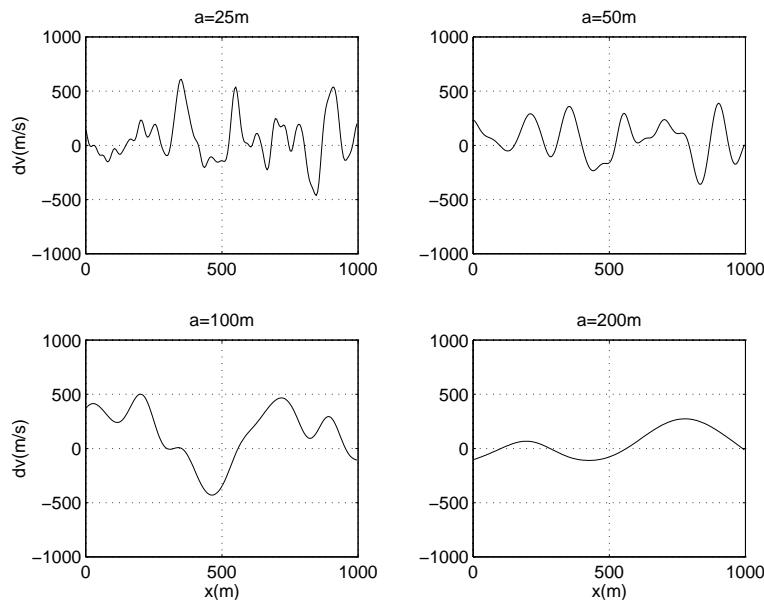


Figure 8. Velocity perturbation profile with correlation lengths $a=25, 50, 100, \& 200m$

Figure 9 is a snapshot in time of a scattered wave field calculated with the finite difference method. The wave is emitted from the source at the surface (depth=0 m), propagates downward,

is reflected by the heterogeneous layer (depth=500 m), and is finally received at the surface. In the figure we see that the primary reflected wave amplitude does not vary smoothly with offset, and there are many later arrivals due to wave scattering.

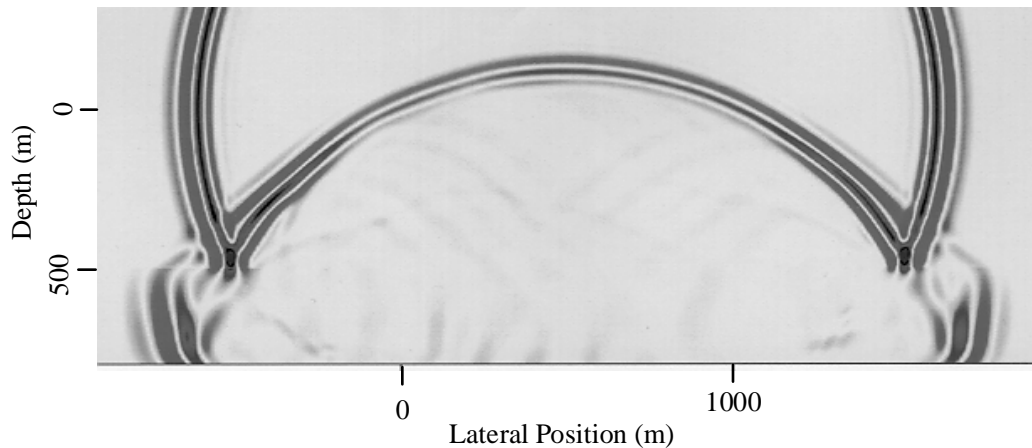


Figure 9. Snapshot of the wave field for heterogeneity with correlation length=50 m

For sources at different lateral positions on the surface, reflected wave amplitudes vary due to wave interactions at the heterogeneous layer. The wave amplitude variations contain information about the heterogeneity scale of the layer. Therefore, we calculate the spatial correlation function between the zero-offset wave amplitudes for sources across the surface.

Characterizing the spatial auto-correlation of the reflected seismic waves measured at the surface is somewhat subjective. Although the wave fields fluctuate spatially due to the model heterogeneity, defining and measuring the fluctuations in different ways produce different spatial auto-correlation functions. The fluctuation of wave fields can be calculated in terms of, the AVO response, the amplitude of the zero-offset reflections, or the stacked reflections. To calculate a wavelet amplitude, time windows of various lengths and positions can be applied to either select the whole reflected wavelet or just its coda. Because the model heterogeneity affects the amplitude of these signals to different degrees, their spatial variations will differ, resulting in different auto-correlation functions.

We first examine the effect of stacking on the spatial auto-correlation function of the reflected waves. Stacking is applied to field data to help stabilize migration calculations, it removes measurement noise and high wave-number features corresponding to small-scale heterogeneity. In our synthetic data the signals are essentially noise-free, therefore, we expect the zero-offset reflection to be similar to the stacked reflection for any given CDP.

In Figure 10 is a comparison of the surface wave field spatial auto-correlation using reflected waves for various numbers of stacks. In the first column are lateral profiles of the reflection amplitudes which are the root-mean-squares of the reflected wavelets. In the second column are the spatial auto-correlations. For auto-correlation calculations on finite data sets (such as these) there is a loss of accuracy for the correlation values at higher spatial lags. Comparing plots from

this figure we see that the stacking has little visible effect on the wave field spatial auto-correlation function. Therefore, for the rest of this work, we use only the zero-offset reflections.

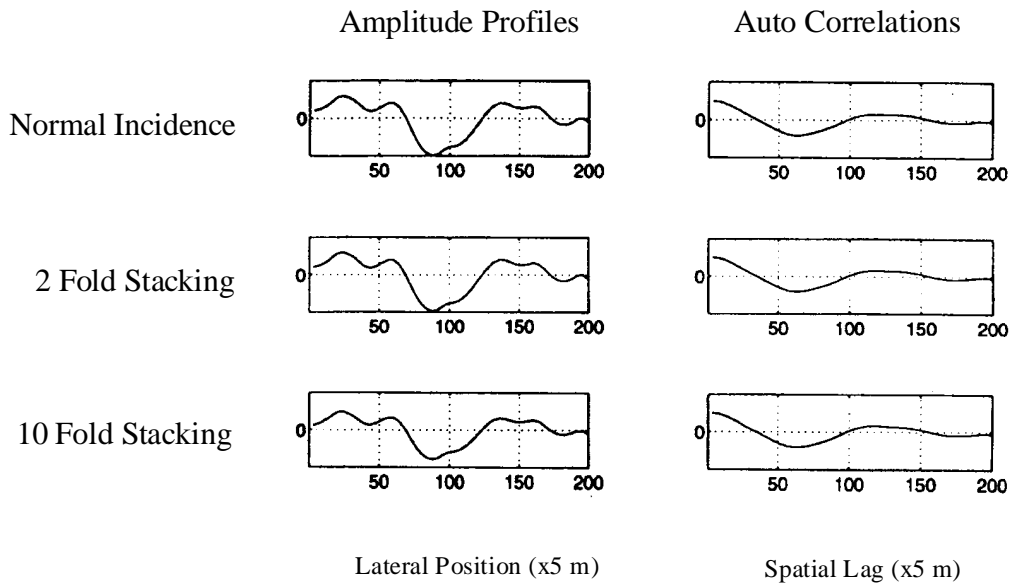


Figure 10. Comparison of reflection amplitude profiles and their spatial auto-correlations for various stacking

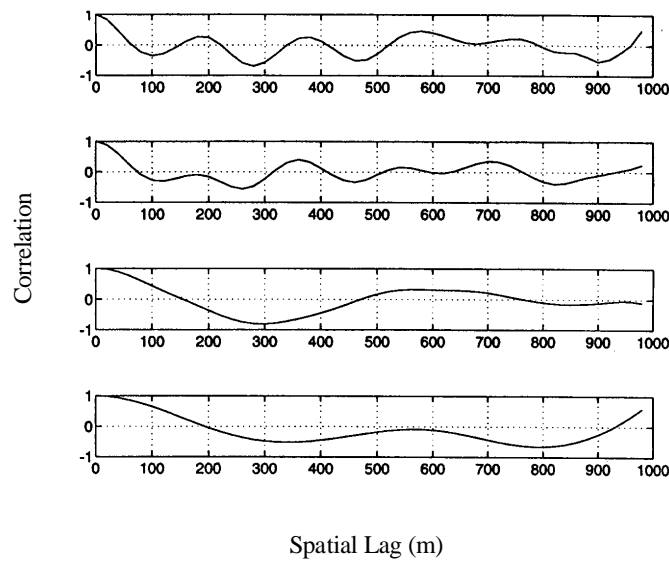


Figure 11. Spatial auto-correlation functions of whole wavelet amplitudes, for models with auto-correlation lengths of 1/4, 1/2, 1 and 2 wavelengths respectively

Figure 11 shows the surface wave field spatial auto-correlation functions for reflected waves from the heterogeneous layer having velocity variations with auto-correlation lengths of 25 m, 50 m, 100 m and 200 m.

It is found that the auto-correlation of the surface wave-field approximates the auto-correlation of the velocity heterogeneity for scales much larger than a wavelength. For heterogeneity of scales near or smaller than the wavelength, the auto-correlation length of the surface wave-field remains around one wavelength. Looking at amplitude variations directly, or deconvolving the reflection seismograms prior to the correlating may reveal the details of "short-wavelength" spatial heterogeneities.

The reflected wavelets are distorted by multi-scattering in the heterogeneous medium, these scattered waves are delayed, and cause distortion to the later part of the wavelet. Therefore, we expect that the amplitude of the coda part of the reflected wavelet should be more sensitive to model heterogeneity than the whole wavelet. Based on this fact, we adjust the time window, to calculate the amplitudes of the coda. The resultant spatial surface wave-field auto-correlation is shown in Figure 12.

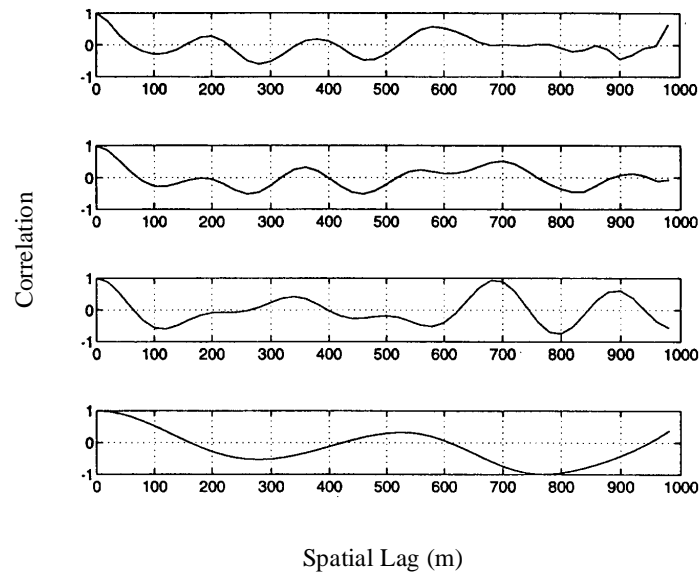


Figure 12. Spatial auto-correlation functions of coda amplitudes, for models with auto-correlation lengths of 1/4, 1/2, 1 and 2 wavelengths respectively

Comparing the auto-correlation plots for heterogeneity at the scale of one wavelength (third from the top) in each of Figures 11 and 12, the auto-correlation of coda data approximates that of the velocity model better. When the coda portion of the signal is isolated, the spatial sensitivity is improved for heterogeneity scales near and less than one wavelength.

Discussion

Science Research Laboratory together with MIT's Earth Resources Laboratory are currently conducting DOE sponsored research to develop numerical techniques for the identification and characterization of fractures in otherwise low permeability natural gas reservoirs. As part of this program, we examine seismic waves scattered from anisotropic heterogeneity with data produced from laboratory ultrasonic models and numerical models. Results from these tests show that in certain cases P-wave AVOA may contain more information than is currently used in common practice. Further, experiments and calculations demonstrate that the lateral correlation of reflected wave amplitudes does depend closely on the model heterogeneity scale producing variability in AVO results which can be an indicator of fracture density and orientation.

Future Activity

The objective of the current program is to produce a modeling technique capable of inverting seismic data sets collected over fractured reservoirs with a wide range of characteristics. The inversion output will contain reservoir characteristics such as alignment, degree and extent of the anisotropy which is directly correlated to fracturing. To accomplish this goal we are continuing development of fast forward modeling algorithms validated with reflection data from the ultrasonic laboratory models, finite difference calculations and analysis of well characterized field data. The laboratory ultrasonic models will be extended to simulate more cases and have greater complexity. The finite difference calculations will be extended to 3D cases to accommodate this additional complexity. As confidence in our forward modeling develops we will be applying these algorithms to field data sets from areas with independent data on fracture characteristics.

Acknowledgments

This research is sponsored by the U.S. Department of Energy's Morgantown Energy Technology Center (METC), under Grant No. DEFG02-95ER82066, High Resolution Seismic Modeling and Analysis of Fractured Reservoirs. We thank William Gwilliam, METC, DOE, for his support and leadership in this project, and John Queen, Conoco, for his valuable insights and guidance.

References

- Aki, K., Richards, P.G., 1980. Quantitative seismology theory and methods, W.H. Freeman and Company, New York
- Bamford, D. and Nunn, K.R., 1979, In situ seismic measurements of crack anisotropy in the Carboniferous limestone of Northwest England, *Geophys. Prosp.*, **27**, 322-338.
- Brekhovskikh, L.M., Godin, O.A., 1990. Acoustics of layered media I, Springer-Verlag, New York
- Castagna, J.P., 1993a. AVO analysis - tutorial and review, *in* Offset-dependent reflectivity - Theory and practice of AVO analysis, Society of Exploration Geophysicists, Investigations in Geophysics Series, Volume 8, 3-36.

- Castagna, J.P., Batzle, M.L. and Kan, T.K., 1993b. Rock physics - the link between rock properties and AVO response, *in* Offset-dependent reflectivity - Theory and practice of AVO analysis, Society of Exploration Geophysicists, Investigations in Geophysics Series, Volume 8, 135-171.
- Cheng, N., 1994. Borehole wave propagation in isotropic and anisotropic media: three-dimensional finite difference approaches, PhD Thesis, MIT.
- Crampin, S., 1981, A review of wave motion in anisotropic and cracked elastic media, *Wave Motion*, **3**, 343-391.
- Crampin, S., McGonigle, R. and Ando, M., 1986, Extensive-dilatancy anisotropy beneath Mt. Hood, Oregon and the effect of aspect ratio on seismic velocities through aligned cracks, *J. Geophys. Res.*, **91**, 12703-12710.
- Gibson, Jr., R.L. and Theophanis, S., 1996. Ultrasonic and numerical modeling of reflections from azimuthally anisotropic media, SEG 66th Annual Meeting, Expanded Abstracts, 1025-1028.
- Gibson, Jr., R.L. and A. Ben-Menahem, 1991. Elastic wave scattering by anisotropic obstacles: application to fractured volumes, *J. Geophys. Res.*, **96**, 19905-19924.
- Hudson, J.A., 1980. Overall properties of a cracked solid, *Math. Proc. Camb. Phil. Soc.*, **88**, 371-384.
- Hudson, J.A., 1981. Wave speeds and attenuation of elastic waves in material containing cracks, *Geophys. J. R. astr. Soc.*, **64**, 133-150.
- Krautkramer, J., Krautkramer, H., 1990. Ultrasonic testing of materials, Springer-Verlag, New York
- Leary, P.C., Li, Y.-G., and Aki, K., 1987, Observation and modeling of fault-zone fracture seismic anisotropy - I. P, SV, SH travel times, *Geophys. J. R. astr. Soc.*, **91**, 461-484.
- Lynn, H.B., Bates, C.R., Simon, K.M., Van Dok, R., 1995. The effects of azimuthal anisotropy in P-wave 3-D seismic, SEG 65th Annual Meeting, Expanded Abstracts, 727-731.
- Mandal, B. and Toksöz, M.N., 1990. Computation of complete waveforms in general anisotropic media - results from an explosion source in an anisotropic medium, *Geophys. J. Int.*, **103**, 33-45.
- Perez, M.A., and Gibson, Jr., R.L., 1996. Detection of fracture orientation using azimuthal variation of P-wave AVO responses: Barinas field (Venezuela), SEG 66th Annual Meeting, Expanded Abstracts, 1353-1356.
- Schoenberg, M. and Douma, J., 1988, Elastic wave propagation in media with parallel fractures and aligned cracks, *Geophys. Prosp.*, **36**, 571-590.
- Sinclair, A.N., Graf, M., Allen, A.L., 1989, Mechanical wave interaction at a diffuse interface, *Research in Nondestructive Evaluation*, **1**, no. 1.
- Zoback, M.L. and Zoback, M., 1980, State of stress in the conterminous United States, *J. Geophys. Res.*, **85**, 6113-6156.